

Quantum Phase Transitions and Persistent Currents in Josephson-Junction Ladders

Minchul Lee

*Department of Physics, Seoul National University, Seoul 151-747, Korea and
Department of Physics, Korea University, Seoul 136-701, Korea*

Mahn-Soo Choi*

Department of Physics, Korea University, Seoul 136-701, Korea

M.Y. Choi

*Department of Physics, Seoul National University, Seoul 151-747, Korea and
Korea Institute for Advanced Study, Seoul 130-012, Korea*

In this work we study quantum phase transitions and persistent currents in capacitively coupled one-dimensional Josephson-junction arrays. We will focus particularly on the roles of exciton-like pairs in the strong coupling limit in the presence of external gate charges and magnetic fluxes. We use the numerical density-matrix renormalization group method for the study in the full range of values of gate charge and magnetic flux. To clarify the various effects, we report the pair correlation functions and the exciton densities as well as the persistent current.

PACS numbers: 74.50.+r, 67.40.Db, 73.23.Hk

I. INTRODUCTION

Systems of Josephson junctions between small superconducting grains have been attracting considerable interest for more than two decades. One of the main attractive features is that they exhibit manifestations of various phenomena in diverse fields of condensed-matter physics. A popular example in contemporary mesoscopic physics is the Coulomb blockade effect and single charge (electron or Cooper pair) tunneling.^{1,2} Persistent current, another hot topic in mesoscopic physics, can also be embodied in Josephson-junction systems. Since the superconducting coherence is easily maintained over a macroscopic length scale, a “necklace” of Josephson junctions (i.e., one-dimensional periodic array of Josephson junctions) may be a good testbed for persistent currents.³ Moreover, charge fluctuations present in such systems may induce quantum phase transitions,^{4,5,6,7,8} providing a prototype model for the noble many-body phenomena in strongly correlated electron systems.⁹ Another important and appealing feature of the systems is the experimental tunability: They not only make mesoscopic devices on their own^{2,10} but also allow us to test and understand otherwise very subtle points of interacting many-particle systems,⁹ which is important from a fundamental point of view.

Here we consider a particular geometry of Josephson-junction systems: a ladder of two capacitively coupled one-dimensional (1D) Josephson-junction arrays. In the Coulomb blockade regime, a single charge cannot tunnel across the junction since it is energetically unfavorable. Transport is therefore dominated by more complex elementary processes that involve several charge-tunneling events. For the particular type of coupling through large inter-array capacitances, the relevant elementary process in the absence of the gate charge consists of cotunnel-

ing of bound pairs of excess and deficit charges, which we call “particles” (excess charges) and “holes” (deficit charges), respectively.¹¹ It was first demonstrated on capacitively coupled normal-metal tunneling junctions^{12,13} and later on superconducting junction arrays.^{14,15} In the presence of gate voltage applied between the electrode islands and the substrate, the particle-hole symmetry is broken and the particle-hole pair no longer makes the lowest charging-energy configuration. For example, when the particle-hole symmetry is broken maximally (corresponding to the gate charge given by one half of the elementary charge $2e$), the transport is governed by cotunneling of particle-void pairs (with the *void* denoting the absence of any excess or deficit Cooper pair).¹⁴ It is noted that these particle-hole pairs or particle-void pairs are reminiscent of *excitons*, i.e., bound states of a band electron and a hole, in solids. In the previous work,¹⁴ quantum phase transitions induced by the cotunneling of particle-hole pairs and particle-void pairs near the particle-hole symmetry line and the maximal-frustration line, respectively, have been studied by means of perturbative methods. However, properties of the transport or phase transitions in between have not been studied.

Effects of an external magnetic flux threading the loop of a ladder of two capacitively coupled Josephson-junction necklaces (CCJJs) (see Fig. 1) are even more sophisticated since the objects involved in the persistent current are not single charges. Unlike most studies of the persistent current (or equivalently, the underlying Aharonov-Bohm effect), which focus on single-charged particles, recent researches into a nano-structure with non-simply-connected geometry have demonstrated¹⁷ that excitons can contribute to persistent currents, in spite of their charge neutrality. The nonvanishing persistent currents in the system, is attributed to the finite probability of breaking and recombination of an exciton via intermediate single particle/hole states. It is

thus quite intriguing to investigate persistent currents in CCJJsNs, where cotunneling of the particles and holes of Cooper pairs dominates the transport phenomena. Additional advantage of the CCJJsNs is that the particle-hole or particle-void pairs are stable while the excitons in semiconductor nano-rings usually have a finite and short life time. Notice further that the CCJJsNs are already within the reach of experimental realization.¹⁵

In this work we study quantum phase transitions and persistent currents in a ladder of CCJJsNs. We focus particularly on the roles of “excitons” in the presence of the charge frustration due to an external gate voltage and the magnetic frustration due to an external magnetic flux threading the necklaces. We use the numerical density-matrix renormalization group (DMRG) method¹⁸ to probe the full ranges of the gate charge and the magnetic flux. Although we are mainly interested in the strong-coupling limit, we will consider for comparison both the two limiting cases: decoupled and strongly coupled cases. In the limit of strong coupling, we identify two different superfluid phases, characterized by condensation of either particle-hole pairs or particle-void pairs, depending on the gate charge. In order to disclose properties of the superfluid phases and formation of excitons explicitly, we measure the pair correlation function and the exciton density. The behavior of the persistent current calculated for small systems reveal the transport via the separation and recombination process for small Josephson energies. At larger Josephson energies, however, the transport is governed by mixing of low-lying charge states with higher-energy states. Finally, we propose an experimentally realizable system to demonstrate the cotunneling process of excitons. The intermediate coupling regime is also interesting and more feasible experimentally.¹⁵ Unfortunately, however, the numerical DMRG study in this case is beyond the current computing power, requiring far more memory than available. We thus leave the intermediate region for the future study.

The remaining part of this paper is organized as follows: In Sec. II we first describe the model Hamiltonians and discuss qualitatively the relevant low-energy charge states. Quantum phase transitions in a single Josephson-junction necklace and capacitively coupled Josephson-junction necklaces are examined in Sec. III. Section IV is devoted to the investigation of the persistent currents in the system, revealing the AB effect of excitons. Finally, we summarize the main results in Sec. V.

II. MODEL

We consider two 1D periodic arrays, which we call *necklaces*, of N superconducting grains as shown in Fig. 1. Any two nearest-neighboring grains on one necklace form a Josephson junction of coupling strength E_J . The two necklaces are coupled with each other via capacitance C_I between corresponding grains, to form a “ladder”. Uniform gate voltage V_g is applied to each grain

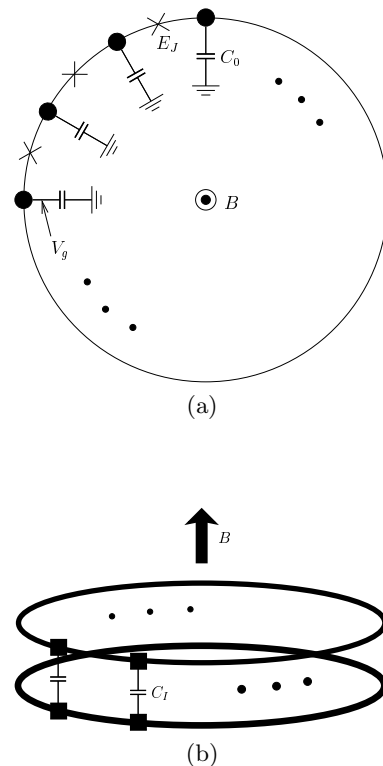


FIG. 1: Schematic diagrams of (a) a single Josephson-junction necklace (from above) and (b) two capacitively coupled necklaces (from the diagonal direction). In (b) each thick ring represents the single necklace depicted in (a).

through its self-capacitance C_0 , inducing gate charge $Q = C_0 V_g$ on each grain. For convenience, we measure the charge in units of $2e$, and write $Q \equiv 2en_g$. In addition, a transverse magnetic flux threads each necklace. Such a system is described by the Hamiltonian

$$\mathcal{H} = 2e^2 \sum_{lx, l'x'} [n_x^l - n_g] C_{lx, l'x'}^{-1} [n_{x'}^l - n_g] - E_J \sum_{lx} \cos(\phi_x^l - \phi_{x+1}^l - A_x), \quad (1)$$

where the number n_x^l of the Cooper pairs and the phase ϕ_x^l of the superconducting order parameter at site x on the l th necklace ($l = 1, 2$) are quantum-mechanically conjugate variables: $[n_x^l, \phi_{x'}^l] = i\delta_{l, l'}\delta_{x, x'}$. The bond angle A_x is given by the line integral of the vector potential \mathbf{A} introduced by the applied magnetic field:

$$A_x = \frac{2\pi}{\Phi_0} \int_x^{x+1} dl \cdot \mathbf{A} = \frac{2\pi f}{N}, \quad (2)$$

where f denotes the total flux in units of the flux quantum $\Phi_0 \equiv 2\pi\hbar c/2e$. Assuming that junction capacitances are negligible, we write the capacitance matrix $C_{lx, l'x'}$ in the form¹⁶

$$C_{lx, l'x'} = [C_0\delta_{l, l'} + C_I(2\delta_{l, l'} - 1)]\delta_{x, x'} \equiv C_{ll'}\delta_{x, x'} \quad (3)$$

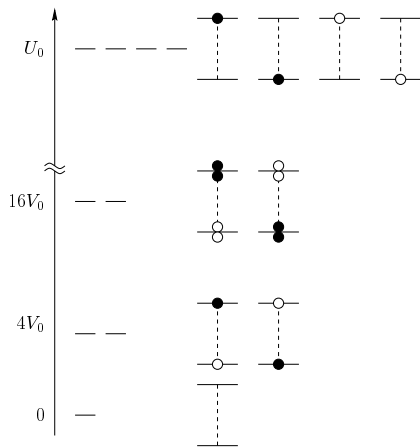


FIG. 2: Energy levels of the charging energy part in Eq. (5) and corresponding charge configurations near the particle-hole symmetry line. Filled and empty circles denote particles and holes, respectively; paired (upper and lower) solid lines represent the two coupled arrays, the couplings between which are illustrated by the dashed lines. The low-lying energy levels satisfying $n_x^+ = 0$ are well separated by a large amount of energy (of the order of E_0) from those with $n_x^+ \neq 0$.

and also define charging energy scales $E_0 \equiv e^2/2C_0$ and $E_I \equiv e^2/2C_I$, associated with the corresponding capacitances. Notice that when $n_g = 0$ the Hamiltonian in Eq. (1) is symmetric with respect to the particle-like (excess Cooper pairs) excitations and hole-like (deficit pairs) ones. On the other hand, charges on each grain are maximally frustrated when $n_g = 1/2$. For later use, we thus name the lines corresponding to $n_g = 0$ and $n_g = 1/2$ the particle-hole symmetry line and the maximal-frustration line, respectively, in the phase diagram.

For the DMRG analysis, we represent the Hamiltonian in Eq. (1) in the boson number basis. Based on the commutation relation between the number n_x^l and the phase ϕ_x^l , we identify the boson creation operator $b_x^{l\dagger}$ at site x on necklace l with $e^{i\phi_x^l}$. In terms of the boson operators, we thus obtain the Bose-Hubbard Hamiltonian

$$\mathcal{H}_{BH} = \frac{8E_0}{2} \sum_{ll'x} n_x^l C_0 C_{ll'}^{-1} n_x^{l'} - 8E_0(n_g + \bar{n}) \sum_{lx} n_x^l - \frac{E_J}{2\bar{n}} \sum_{lx} \left(e^{-2\pi i f/N} b_x^{l\dagger} b_{x+1}^l + h.c. \right), \quad (4)$$

where \bar{n} is the average boson number per site. Note that in the quantum phase model the Josephson energy term is independent of the number fluctuations, while the corresponding (hopping) term is not in the Bose-Hubbard model. To alleviate the effects of number fluctuations in the Bose-Hubbard model, we consider the case that the average boson number \bar{n} per site is large¹⁹: Throughout this study we set \bar{n} to be 10000.

Capacitive coupling between necklaces drastically affects the low-lying charge excitations, especially, in the

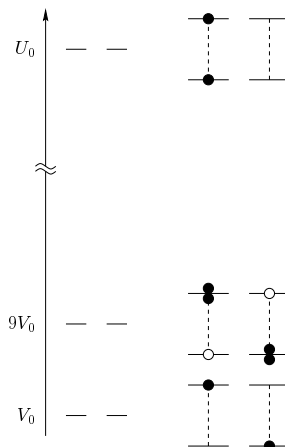


FIG. 3: Energy levels and corresponding charge configurations near the maximal-frustration line. Note that the ground state is two-fold degenerate per site.

strong coupling regime. To examine the charge configurations in the low-lying states, it is convenient to rewrite the charging energy part in the Hamiltonian (4):

$$\mathcal{H}_{BH} = U_0 \sum_x (n_x^+ - 2n_g)^2 + V_0 \sum_x (n_x^-)^2 - \frac{E_J}{2\bar{n}} \sum_{lx} \left(e^{-2\pi i f/N} b_x^{l\dagger} b_{x+1}^l + h.c. \right), \quad (5)$$

where we have defined new energy scales $U_0 \equiv 2E_0$ and $V_0 \equiv 2E_0/(1 + 2C_I/C_0)$ and charge variables $n_x^\pm \equiv (n_{1,x} - \bar{n}) \pm (n_{2,x} - \bar{n})$. Note that n_x^\pm represents the total number of (excess) Cooper pairs on the x th rung of the ladder. In the regime of concern ($C_I \gg C_0$, i.e., $E_I \ll E_0$), we have $U_0 \gg V_0$ and $U_0 \gg E_J$, and the charge configurations satisfying $n_x^+ - 2n_g \simeq 0$ are thus strongly favored. In such a charge configuration $n_x^-/2$ corresponds to the number of excitons (particle-hole or particle-void pairs, see below).

The representation in Eq. (5) of the Hamiltonian allows us to distinguish clearly the two interesting regions from each other: near the particle-hole symmetry line ($n_g = 0$) and near the maximal-frustration line ($n_g = 1/2$), as one can observe from the energy spectra of the charging energy part illustrated in Figs. 2 and 3 for the two regimes, respectively. Near the maximal-frustration line, the charge configurations that do not satisfy the condition $n_x^+ = 1$ (for all x) have a huge excitation gap of the order of E_0 . Furthermore, the ground states of the charging energy part, separated from the excited states by a gap of the order of E_I , have two-fold degeneracy for each x , corresponding to $n_x^- = \pm 1$. Near the particle-hole symmetry line, on the other hand, low-energy charge configurations should satisfy the condition $n_x^+ = 0$ for all x . Unlike the former case, the ground state of the charging energy is non-degenerate and forms a Mott insulator characterized by $n_{1,x} = n_{2,x} = 0$ for all x . As E_J is turned on, the ground state is mixed with the states with

$n_x^- = \pm 2$. In the intermediate region ($0 < n_g < 1/2$), these two kinds of energy spectra are interleaved to form a complex shape of the energy levels.

III. QUANTUM PHASE TRANSITIONS

The competition between charge order and phase coherence gives rise to quantum fluctuations and quantum phase transitions at zero temperature. For large charging energy ($E_0 \gg E_J$), the bosons become localized and the system is in the Mott insulator phase with integer density. On the contrary, for large hopping energy or Josephson energy ($E_J \gg E_0$), coherence of the phases ϕ_x dominates over the system and the superfluid (SF) region with delocalized bosons is observed. The properties and universality classes of the phase transitions, however, depend strongly on the coupling strength C_I/C_0 as well as the chemical potential $\mu \equiv 8E_0(n_g + \bar{n})$. The charge frustration n_g may be restricted to the range $[1, 1/2]$ since the Hamiltonian in Eq. (5) is periodic in n_g with period unity and has reflection symmetry about the $n_g = 1$ (or any integer) line. In the followings we investigate two limiting cases: the decoupled case ($C_I = 0$) and the strongly coupled one ($C_I \gg C_0$).

A. Single Josephson-junction necklace

The phase transition in a single Josephson-junction array has been studied quite extensively and it has been found that its nature depends crucially on the gate voltage. In the presence of nonzero gate voltage ($n_g \neq 0$), the density of the system changes as the phase boundary is crossed from the incompressible insulator to the compressible superfluid. The transition can thus be located at the point where in the thermodynamic limit the density of the ground state becomes different from one of the insulator ground state as the Josephson energy is increased. On the other hand, in the particle-hole symmetry line ($n_g = 0$), the density remains to be an integer at the phase transition. Therefore, in this case the phase boundary is determined by the single-particle excitation gap. This is possible because in the superfluid phase the ground state is a superposition of states with different boson numbers, the energy gap between the ground state and the states with additional particles, which is finite in the insulating phase, vanishes in the superfluid phase.

Since the Hamiltonian conserves total charge number, the DMRG algorithm can be set up to target states with given total excess number M of bosons. We thus obtain the phase diagram of the system by comparing energies of the ground states with different boson numbers: the energy $E_{M=0}$ of the insulator ground state with zero excess boson density ($\langle n_x \rangle = \bar{n}$) and the energy $E_{M=1}$ of the eigenstate with an additional particle upon the ground state. Through the linear extrapolation of the energy gap $E_{M=1} - E_{M=0}$ for finite system size $N = 64, 128, \text{ and } 256$,

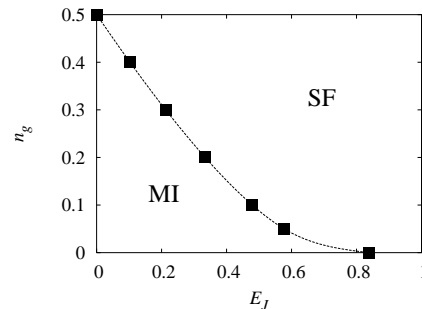


FIG. 4: Phase diagram for a single 1D Josephson array. The phase boundary separates the Mott insulator (MI) with zero excess Cooper pair density from the superfluid phase (SF). The Josephson energy E_J is expressed in units of $8E_0$ and the error bars in the E_J direction (for given n_g) are smaller than the square symbols. The line is merely a guide to the eye.

we have estimated the gap in the thermodynamic limit and located the phase boundary at the point where the gap is zero. For high numerical accuracy and access to large systems, the finite-size DMRG algorithm and open boundary conditions have been used. During the DMRG process, the boson number at each site is truncated to be less than six and the discarded weight is set to be less than 10^{-6} , giving rise to negligible errors in the gap energy.²⁰ The magnetic frustration f is set equal to zero because it can be gauged away and becomes irrelevant in the thermodynamic limit.

Figure 4 displays the resulting phase diagram for the quantum phase model on the E_J - n_g plane, in the range $0 \leq n_g \leq 1/2$ and $0 \leq E_J \leq 8E_0$. For convenience, here and in all subsequent figures, the energy is expressed in units of $8E_0$. The phase diagram, where the Mott insulator region with zero excess boson density is separated from the compressible superfluid, is in good agreement with those obtained via the perturbative expansion²¹ and the quantum Monte Carlo method.²² On the particle-hole symmetry line the quantum phase model is mapped exactly to the (1+1)-dimensional XY model, predicting a Beresenskii-Kousterlitz-Thouless (BKT) transition²³ driven purely by phase fluctuations. The sharp-pointed shape of the insulating region near the symmetry line reflects the slowness in closing the energy gap in the BKT transition.²⁰ In case that the particle-hole symmetry is broken (away from the symmetry line), no such slowness is found and the commensurate-incommensurate transition belongs to a universality class other than that of the XY model, with different critical exponents²² and RG characteristics.²⁴

B. Strongly coupled Josephson-junction necklaces

In the strong coupling limit, the low-energy charging states relevant to the phase transition are the the

particle-hole pairs (with $n_x^+ = 0$ and $n_x^- = \pm 2$) and the particle-void pairs (with $n_x^+ = 1$ and $n_x^- = \pm 1$). For small hopping strength, these excitons are localized and the system is in the Mott insulator phase. As E_J increases, the phase boundary is crossed from the insulator to the superfluid which, in this case, originates from condensation of the excitons. Accordingly, as in the case of a single Josephson-junction necklace, the transition can be located as one tracks the energy taken to add an exciton to the insulator: At the phase boundary this energy vanishes in the thermodynamic limit. Which kind of exciton between the particle-hole pair and the particle-void pair is relevant depends on the charge frustration n_g . Near the particle-hole symmetry line ($n_g \approx 0$), the particle-hole pairs are energetically favorable and governs the phase transition. As n_g is increased and in the presence of the Josephson tunneling, in contrast, the particle-void pairs begin to be dominant faster than the particle-hole pairs, which will be shown below.

In the DMRG procedure we have associated the target state with a pair of total excess boson numbers (M_1, M_2) on the two arrays by utilizing the boson number conservation. In order to locate the phase boundary, we have calculated the energy $E_{(M_1, M_2)}$ of three kinds of eigenstate: the insulator ground state with $(M_1, M_2) = (0, 0)$ and the states with additional particle-hole and particle-void pairs upon the ground state, labeled by $(M_1, M_2) = (1, -1)$ and $(1, 0)$, respectively. We have extrapolated the energy gaps $E_{(1, -1)} - E_{(0, 0)}$ and $E_{(1, 0)} - E_{(0, 0)}$ for finite system size $N = 16, 32$, and 64 to locate the transition points where the gaps vanish in the thermodynamic limit. As in the case of a single Josephson necklace, we have employed the finite-size DMRG algorithm, imposing open boundary conditions.

Figure 5 shows the energy gaps as functions of the Josephson energy at various charge frustrations, in the system with $C_I/C_0 = 100$ and $N = 32$. From Fig. 5(a) we observe that the excitation energy $E_{(1, -1)} - E_{(0, 0)}$ for different charge frustrations collapses into one curve, which also happens at other system sizes. This indicates that the critical Josephson energy at the transition driven by the particle-hole pairs does not depend on n_g . On the other hand, the energy gap $E_{(1, 0)} - E_{(0, 0)}$ decreases almost linearly with the increase of n_g and E_J , as shown in Fig. 5(b). The larger n_g is, the smaller the Josephson energy E_J at which the energy gap vanishes becomes. For $n_g \gtrsim 0.14$, the critical value of E_J become even less than that for the particle-hole pairs.

The resulting phase diagrams for strongly coupled arrays with $C_I/C_0 = 100$ and 200 are exhibited in Fig. 6 (a) and (b), respectively. Based on the dominant transport mechanism, one can distinguish three regions in the superfluid phase: ES₁, ES₂, and SFUB. In region ES₁ the transport is driven mainly by the excitons of particle-hole pairs; in ES₂ it is driven by particle-void pairs. In region SFUB, on the other hand, single-particle processes dominate the transport in the system. Such superfluid of unpaired bosons (SFUB) is to be observed at $E_J/8E_0 \sim 1$,

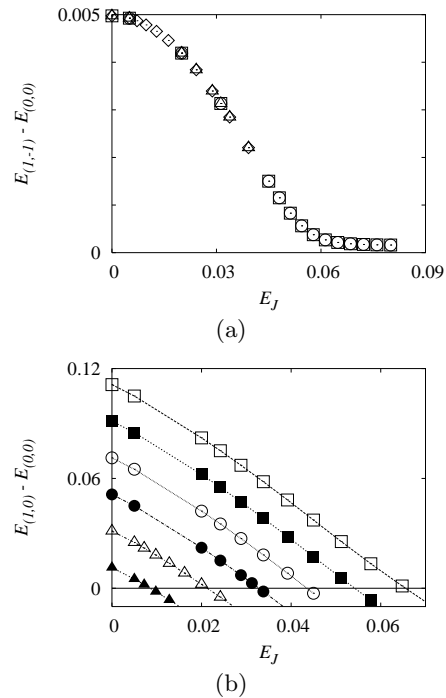


FIG. 5: Energy gaps (a) $E_{(1, -1)} - E_{(0, 0)}$ and (b) $E_{(1, 0)} - E_{(0, 0)}$. Both are taken for $C_I/C_0 = 100$ at the system size $N = 32$. Each symbol corresponds to a different value of charge frustration: (a) $n_g = 0$ (\square), 0.1 (\circ), 0.2 (\triangle), and 0.24 (\diamond); (b) $n_g = 0.14$ (\square), 0.16 (\blacksquare), 0.18 (\circ), 0.2 (\bullet), 0.22 (\triangle), and 0.24 (\blacktriangle). The energies on both axes are expressed in units of $8E_0$.

far to the right from regions ES₁ and ES₂, and not shown in the phase diagram given by Fig. 6. We note that different transport mechanisms take over dominant roles gradually as the control parameters are changed. Therefore, regions ES₁ and ES₂ in Fig. 6 should not correspond to truly distinct phases.

Previous studies on mapping of the system at the particle-hole symmetry line to (1+1)-dimensional system of classical vortices^{25,26} insisted that the system is effectively described by a two-dimensional XY model and exhibits a BKT transition at the critical Josephson energy $E_J/8E_0|_c = 4K_{BKT}^2(1 + \sqrt{1 + 2C_I/C_0})^{-2} \approx 2K_{BKT}^2(C_0/C_I)$, where $K_{BKT} \approx 0.748$ is the critical coupling strength for the standard XY model. Our data, though being unable to discern nature of the transition, show that the critical Josephson energy is inversely proportional to $\sqrt{C_I/C_0}$ instead of C_I/C_0 , apparently favoring against the BKT transition. This result is quite reasonable in view of the fact that the cotunneling process of particle-hole pairs via an intermediate virtual state happens with the probability proportional to E_J^2/E_0E_I , leading to $E_J/E_0|_c \propto \sqrt{C_I/C_0}$. In addition, the nonzero charge frustration does not change the properties of the phase transition abruptly, in contrast to the case of a single array. Instead, the transition point as well as the qualitative properties is preserved up to $n_g \approx 0.135$ for $C_I/C_0 = 100$ and to $n_g \approx 0.165$ for $C_I/C_0 = 200$; there

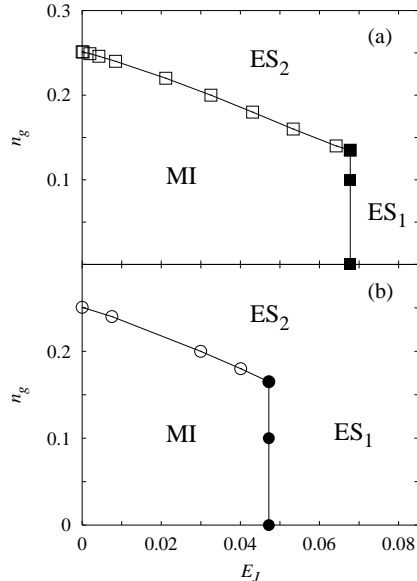


FIG. 6: Phase diagrams for strongly coupled 1D Josephson arrays for (a) $C_I/C_0 = 100$ and (b) $C_I/C_0 = 200$. Displayed are the phase boundaries between the Mott insulator (MI) phase and the superfluid phase (ES₁ and ES₂). Regions ES₁ and ES₂ in the superfluid phase are distinguished by the dominant transport mechanism (see the text). The transitions across the boundaries indicated by filled and empty symbols are driven by the particle-hole pairs and by the particle-void pairs, respectively. The lines are merely guides to eyes.

is no increase in the critical value of E_J as predicted in Ref. 14. Since our model neglects the junction capacitance on each necklace, for

$$n_g > n_g^* \equiv \frac{1}{4} \left(1 + \frac{1}{1 + 2C_I/C_0} \right), \quad (6)$$

each site has two-fold degenerate ground states ($n_x^+ = 1$ and $n_x^- = \pm 1$) of the charging energy. Accordingly, the Josephson energy of any strength brings about charge fluctuations to drive the system into the superfluid phase. Indeed Figure 6 shows that the MI phase ceases to exist for $n_g > n_g^*$, regardless of E_J . With nonzero junction capacitance, the degeneracy is expected to be broken, generating another insulating phase: the charge-density wave (CDW) phase. The perturbative study¹⁴ has found that as the Josephson energy is increased the system goes from the CDW insulator to the Luttinger liquid phase.

To witness the activity of the excitons in the phase transition, we have measured the pair correlation function defined to be

$$C_{pair} \equiv \frac{1}{N} \sum_x \langle (n_x^1 - \langle n_x^1 \rangle)(n_x^2 - \langle n_x^2 \rangle) \rangle \quad (7)$$

together with the exciton density P_0 of the particle-hole

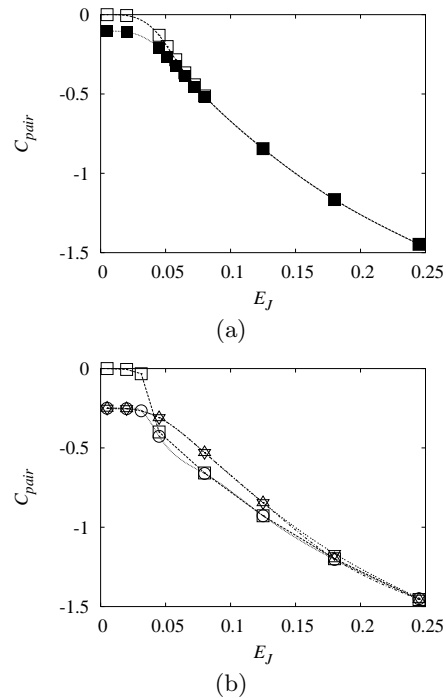


FIG. 7: Pair correlation C_{pair} versus the Josephson energy. (a) For $n_g = 0$, the pair correlation functions in the insulator ground state (empty symbols) and in the state with one particle-hole pair added upon the ground state (filled symbols) are plotted. (b) shows the correlations in the ground state in the presence of the gate voltage $n_g = 0.2(\square)$, $0.3(\circ)$, $0.4(\triangle)$, and $0.5(\nabla)$. Here we set $C_I/C_0 = 100$ and the system size $N = 8$, and lines are guides to eyes.

pairs and $P_{\pm 1}$ of the particle-void pairs:

$$P_0 \equiv \frac{1}{N} \sum_x \langle \delta_{n_x^1 + n_x^2, 0} - \delta_{n_x^1, 0} \delta_{n_x^2, 0} \rangle \quad (8)$$

$$P_{n^+} \equiv \frac{1}{N} \sum_x \langle \delta_{n_x^1 + n_x^2, n^+} \rangle \quad (n^+ \neq 0). \quad (9)$$

The pair correlation function assumes zero if there is no correlation between the boson numbers on the two arrays; a particle-hole or particle-void pair at every site on the average contributes to C_{pair} by -1 or $-1/4$.

Figure 7 shows that the pair correlation is negative and monotonically decreases with E_J , which indicates that larger hopping strength makes more excitons come into the system. For $n_g = 0$ [see Fig. 7(a)], the two pair correlation functions, one for the insulator ground state and the other for the state with an additional particle-hole pair, approach each other and collapse at $E_J/8E_0 \gtrsim 0.07$, giving another evidence for the condensation of excitons. For $n_g = 0.2$, the correlation changes abruptly at the phase transition, as shown in Fig. 7(b). For $n_g \geq 0.3$, we have $C_{pair} \approx -1/4$ for small values of E_J , which reflects the contribution of particle-void pairs. Although the correlations for $n_g \geq 0.3$ become similar at large values of E_J , they do not coincide at intermediate values, implying

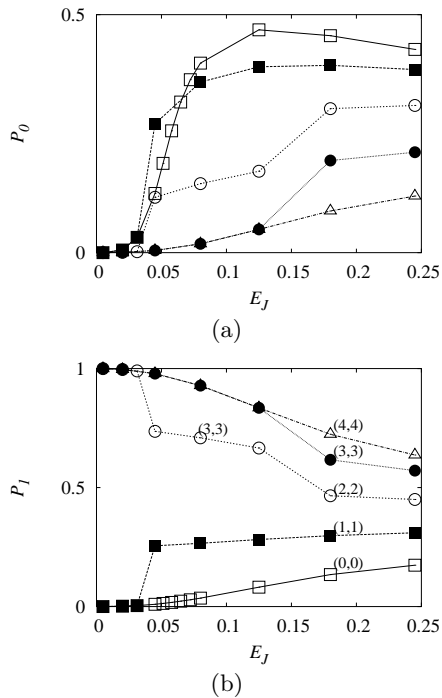


FIG. 8: Exciton densities (a) P_0 and (b) P_1 versus the Josephson energy for gate voltage $n_g = 0(\square)$, 0.2(\blacksquare), 0.3(\circ), 0.4(\bullet), and 0.5(\triangle). Other parameters are the same as those in Fig. 7. The pairs of numbers (M_1, M_2) represent the total excess boson numbers of the ground state at given parameters.

the difference in the history of pair generation.

The behavior of the exciton density with E_J , displayed in Fig. 8, manifests more clearly the formation of the excitons. The particle-hole pair density P_0 grows with E_J [see Fig. 8(a)], except for the case of $n_g = 0$ and large E_J . On the other hand, Fig. 8(b) shows that the density P_1 of the particle-void pairs with $n_x^1 + n_x^2 = 1$ has two kinds of tendencies: For $n_g < n_g^*$ the density P_1 increases with E_J ; otherwise it decreases. The step changes in both densities P_0 and P_1 happens when the total excess boson number $M = M_1 + M_2$ of the ground state is altered. Such behaviors of P_0 and P_1 reveal that more than one kinds of excitons proliferate in the system as E_J is increased beyond its critical value. With large E_J , the kinetic energy gain due to the Josephson tunneling term compensates for the charging energy gap between different kinds of excitons.

We close this section with a comment about the pair correlation in the limit $E_J/8E_0 \gg 1$, which is beyond our current computational power. Our data shows no indication for the decrease of the pair correlation with E_J raised. However, when the Josephson energy is large enough for the single processes of unpaired particles to prevail, the pair correlation may eventually approach zero again.

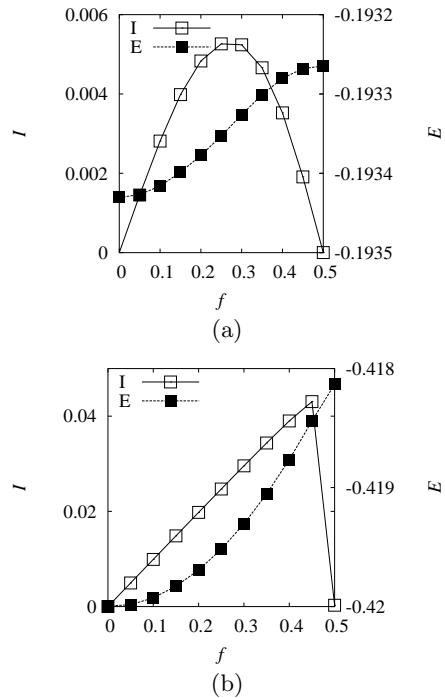


FIG. 9: Persistent current I and ground state energy E as functions of the flux f in (a) the insulating phase ($E_J/8E_0 = 0.64$) and (b) the superfluid phase ($E_J/8E_0 = 1$) along the particle-hole symmetry line ($n_g = 0$).

IV. PERSISTENT CURRENT

In this section we consider the persistent current along the necklaces, induced by the threading external magnetic field. Since tunneling of Cooper pairs between necklaces is not permitted, the persistent current carried by each necklace is given by the derivative of the energy with respect to the magnetic flux f :³

$$I_l = \frac{e}{2\pi\hbar} \left\langle \frac{\partial \mathcal{H}}{\partial f} \right\rangle_l = -\frac{eE_J}{N\hbar n} \text{Im} \left\langle e^{-2\pi i f/N} b_x^\dagger b_{x+1}^l \right\rangle, \quad (10)$$

which is simply the supercurrent through the Josephson junctions. The current in the system is thus given by the imaginary part of $\langle \exp[i(\phi_x^l - \phi_{x+1}^l - A_x)] \rangle$, the real part of which describes the gauge-invariant phase correlation function between nearest neighboring grains. Since the current is periodic in f with period unity and an odd function of the flux f , it is sufficient to calculate the current in the range $f \in [0, 1/2]$. As in the previous section, we focus on two extreme cases: the decoupled case ($C_I = 0$) and strongly coupled one ($C_I/C_0 \gg 1$).

A. Single Josephson-junction necklace

We have calculated the persistent current in a finite-size system ($N = 40$) under periodic boundary conditions. The persistent current is evaluated in the ground

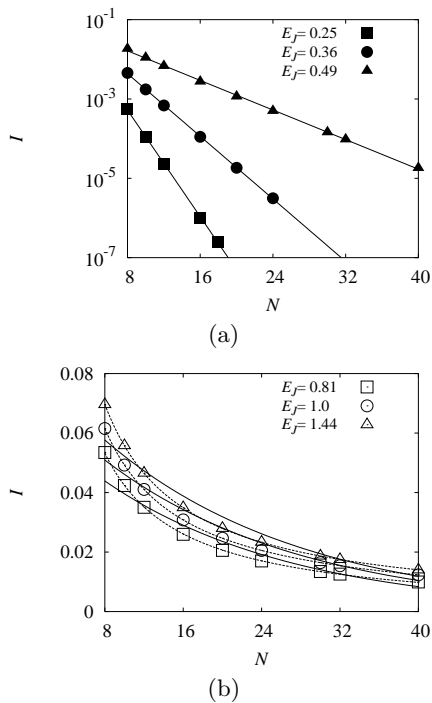


FIG. 10: Persistent current I versus the system size N in (a) the insulating phase [$E_J = 0.25$ (■), 0.36 (●), and 0.49 (▲) in units of $8E_0$] and (b) the superfluid phase [$E_J = 0.81$ (□), 1.0 (○), and 1.44 (△) in units of $8E_0$] along the particle-hole symmetry line ($n_g = 0$). Solid and dotted lines represent the exponential function ae^{-bN} and the algebraic function c/N , respectively, where the constants a , b , and c are obtained via a fitting algorithm.

state, namely, the lowest-energy state, which is found by varying the total excess boson number M at given n_g and E_J , and expressed in units of $eE_J/N\hbar$ in all subsequent figures. Figures 9(a) and 9(b) show the dependence of the persistent current (in units of $eE_J/N\hbar$) and of the ground state energy (in units of $8E_0$) on the flux f in both the insulating phase and in the superfluid phase, respectively, without the gate charge ($n_g = 0$). For small E_J , the current depends sinusoidally on f , whereas it has a saw-tooth shape in the superfluid phase. Such behavior of the persistent current is well known in the two extreme one-dimensional electron models: In the tight-binding model with the lattice potential energy dominant over the kinetic energy, the single-particle energy is given by a cosine function of the flux f , giving rise to sinusoidal dependence of the current on f . On the other hand, the free electron model on a ring, where the energy is quadratic in f , has the persistent current linear in f and of the saw-tooth shape. In our model Cooper pairs take the role of the electrons and in analogy we infer that the saw-tooth dependence in the persistent current indicates the emergence of the superconductivity over the system, where the Cooper pairs can freely move around. Our data for the dependence of the current on the system size, shown in Fig. 10, also leads to the same interpreta-

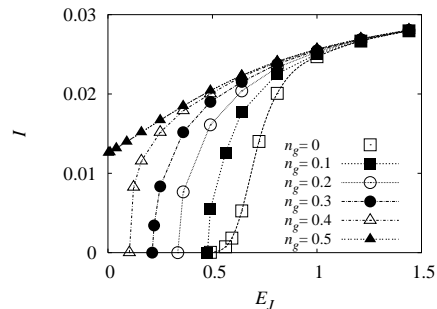


FIG. 11: Persistent current versus the Josephson energy for various gate voltages. In each case the current, scaled in units of $eE_J/N\hbar$, makes clear the contribution of the correlations between nearest-neighboring grains. All the currents are calculated at $f = 1/4$.

tion: In the insulating phase the bosons are localized at sites so that the probability for a boson to circle around the ring and to return to its starting position is proportional to t^N , where t is the hopping probability between nearest neighbors. This gives the current decaying exponentially with the system size N [see Fig. 10(a)]. On the other hand, in the superfluid phase the wave function of the boson is extended and the hopping probability over the system does not depend on the system size. Instead, since the energy itself is quadratic in the system size, the persistent current follows a power-law with respect to the system size, as shown in Fig. 10(b). Hence our data for the persistent current are fully consistent with the phase transition explained in Sec. III A.

We exhibit the dependence of the persistent current on the Josephson energy at $f = 1/4$ and various gate voltages in Fig. 11. The persistent current scaled by E_J is negligibly small in the insulating region, then rises rapidly near the transition point, and increases only marginally in the superfluid phase. For $n_g = 0$, the current shows finite-size effects, gradually increasing quite before the transition point. On the contrary, in the presence of nonzero gate voltage, the current increases very sharply at the phase boundary even in the small-size system, which is attributed to the abrupt change in the total boson number or the density of the ground state at the transition point. Deep in the superfluid phase, on the other hand, the persistent current becomes independent of the gate voltage.

B. Strongly coupled Josephson-junction necklaces

From the observation in Sec. III B, it is evident that in the strongly coupling limit the excitons such as particle-hole and particle-void pairs play dominant roles in the transport. In the picture of the lowest-order cotunneling processes illustrated in Fig. 12, however, such pairs are tightly bound throughout the transport process. Accordingly, the current induced in one necklace is accompanied

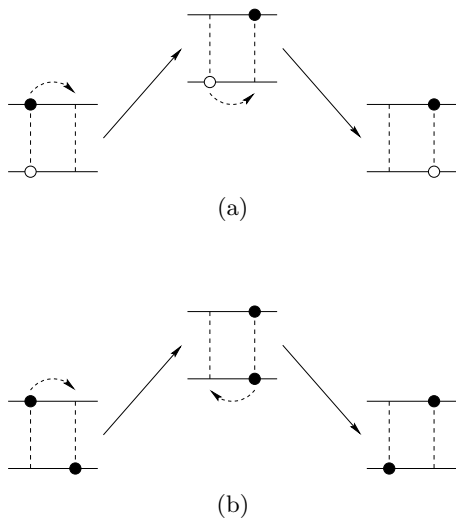


FIG. 12: Typical cotunneling processes relevant (a) near the particle-hole symmetry line and (b) near the maximal-frustration line. Such cotunneling results in the current mirror effects.

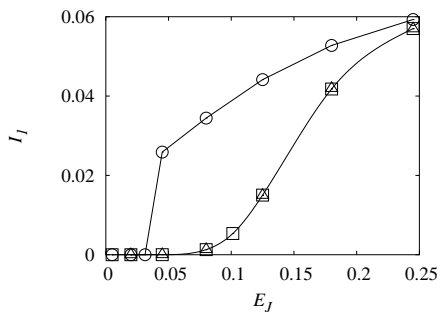


FIG. 13: Persistent current I_1 (along one necklace) versus the Josephson energy E_J in the strongly coupled system of size $N = 8$, for $f = 1/4$ and gate voltage $n_g = 0(\square)$, $0.2(\circ)$, and $0.5(\triangle)$. Lines are merely guides to eyes.

by the secondary current in the other necklace, with the same magnitude but in the opposite direction.¹⁴ On the other hand, in response to the magnetic flux, the charges in an excitonic pair tend to move in opposite directions since their signs are opposite (with respect to the offset charge n_g). Therefore the current mirror effect competes with the influence of the magnetic flux.

Indeed, for small values of the Josephson energy ($E_J/8E_0 \lesssim 0.07$), the persistent current is quite negligible both on the particle-hole symmetry line ($n_g = 0$) and on the maximal-frustration line ($n_g = 1/2$) (see Fig. 13). The small but still non-zero amount of persistent current is induced via higher-order tunneling processes. Namely, the charges in an excitonic pair break up, run down the circumferences in the opposite directions, and recombine. Contributions from these processes are observable only in a system with a small number of sites ($N = 8$ for the data in Fig. 13). In other words, the current mirror effect wins the competition. It is distinguished from the

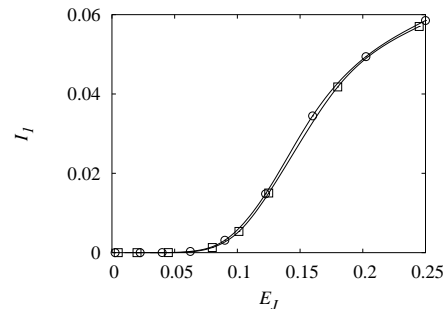


FIG. 14: Persistent current versus the Josephson energy on the particle-hole symmetry line ($n_g = 0$) in the strongly coupled system with the coupling capacitance $C_I/C_0 = 100(\square)$ and $200(\circ)$.

behavior of the persistent current in a single Josephson-junction necklace, where for $n_g = 0$ the current increases rapidly near the transition point and any strength of the Josephson energy induces rather large persistent current for $n_g = 0.5$ (see Fig. 11), demonstrating the action of a different kind of charge fluctuations in the coupled system.

For larger values of the Josephson energy ($E_J/8E_0 \gtrsim 0.07$), however, a considerable amount of persistent current flows through the system and increases with E_J . It can be explained by the generation of excitations with higher charging energies in the presence of the Josephson energy. As observed in Fig. 8, with the increased Josephson energy, more of the charge states that do not satisfy $n_x^+ = 0$ (near the particle-hole symmetry line) or $n_x^+ = 1$ (near the maximal-frustration line) are now mixed with the lowest charging energy states. These excitations can carry a finite amount of persistent current since the signs of the charges in a pair are not opposite now. In short, the magnetic frustration wins the competition with the current mirror effect. It is also interesting that the persistent currents for $n_g = 0(\square)$ and for $1/2(\triangle)$ are almost the same. In fact, the densities of charge excitations which do not satisfy the lowest-charging energy condition are nearly the same for the two cases since the charging energy costs for such excitations amount to the same energy U_0 in both cases.

Note also that unlike these two cases the persistent current for $n_g = 0.2(\circ)$ increases sharply at the transition point and becomes quite larger than the one for $n_g = 0$ or $1/2$. Intermediate values of charge frustration (in the superfluid phase) bring about a variety of charge excitations in the presence of the Josephson energy and diminish the energy gap between the charge excitations, giving rise to the reduction of the current mirror effect and favoring independent single-charge transport.

Figure 14 shows that the persistent current increases slightly as the coupling capacitance is raised. On one hand, a larger value of the coupling capacitance reduces the lowest excitation energy ($\sim E_I$) and makes the excitons more proliferate in the system, thus increasing the

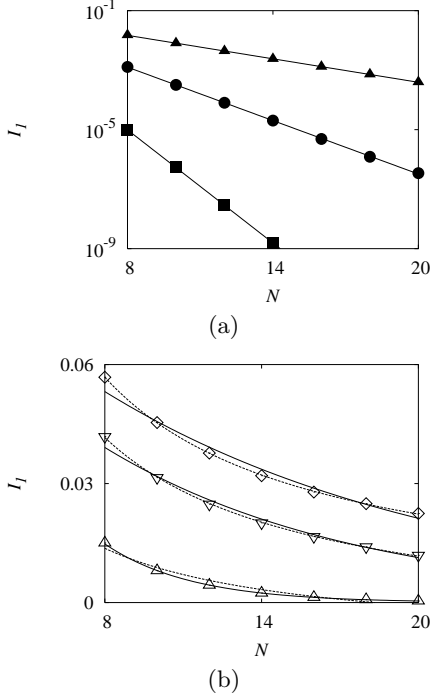


FIG. 15: Persistent current versus the system size on the particle-hole symmetry line ($n_g = 0$) for different values of the Josephson energy $E_J =$ (a) 0.045 (\blacktriangle), 0.08 (\bullet), and 0.125 (\blacktriangle); (b) 0.125 (\triangle), 0.18 (∇), and 0.245 (\diamond) (again in units of $8E_0$). The fitting curves are the same as those given in Fig. 10.

persistent current due to the excitons. On the other hand, breaking of the excitons, which is crucial for inducing the persistent current, costs higher energy ($\sim E_0$). These conflicting trends result in the slight increase in the regime of our interest ($E_0 \gg E_I$).

The dependence of the current on the system size also supports our scheme for the role of the excitons in the persistent current. Figure 15 shows that, similarly to the case of a single necklace, in the insulating phase the current decays exponentially with the system size and decreases inversely to the system size deep in the superfluid phase. Near the transition point on the side of the superfluid phase (at $E_J/8E_0 = 0.08$ and 0.125), however, the current does display exponential dependence on the system size, which indicates that spatially localized objects participate in the generation of the current. It is another evidence for the virtual processes of unpaired charges or higher-order excitons, in the region where the low-lying excitons themselves are delocalized over the system.

To reveal the cotunneling process more explicitly, we devise another interesting configuration that the magnetic field penetrates only one necklace ($l = 1$) without affecting the other ($l = 2$). Such a setup may be realized experimentally as shown in Fig. 16. Notice that only part of the two necklaces are capacitively connected. In order for the persistent current to flow through uncoupled grains, the Josephson coupling between those uncoupled grains should be sufficiently large. In this arrange-

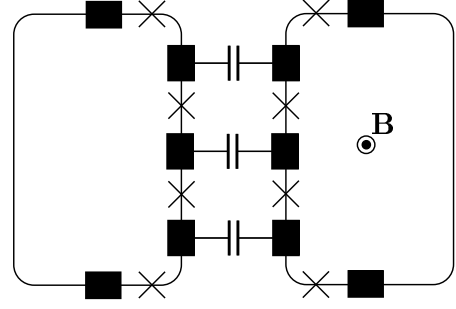


FIG. 16: Schematic diagram of two coupled Josephson-junction necklaces. Part of the two necklaces are capacitively connected whereas the magnetic field threads only one of the two necklaces.

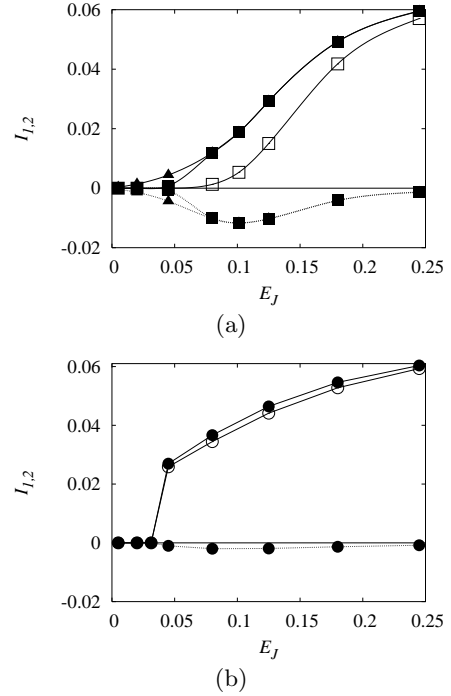


FIG. 17: Persistent currents I_1 (solid lines with filled symbols) and I_2 (dotted lines with filled symbols) when the magnetic field threads only the first ($l = 1$) necklace. The currents are calculated for the gate voltage $n_g =$ (a) 0 (\blacksquare), 0.5 (\blacktriangle); (b) 0.2 (\bullet). For comparison, the persistent currents when both the necklaces are threaded by the magnetic field (see Fig. 13) are also plotted, represented by the corresponding empty symbols.

ment, one can observe the current mirror effect, similar to the case that only one chain is biased by an external voltage.^{13,15}

Figure 17(a) exhibits the current mirror effect in the system with the magnetic field threading only the first ($l = 1$) necklace. On the particle-hole symmetry and the maximal-frustration lines, the two persistent currents I_1 and I_2 along the first and the second ($l = 2$) necklaces, respectively, satisfy the relation $I_1 \approx -I_2$ in the range

$E_J/8E_0 \lesssim 0.07$. As E_J is increased further, nonetheless, not only the mirror effect disappears gradually but also the current I_2 diminishes to zero. It means that the independent single-charge transport rather than the cotunneling transport is favorable at large values of the Josephson energy. Note that the current I_1 is much higher than the corresponding current in the system with the magnetic field acting on both necklaces. Interestingly, unlike the previous setup, the persistent current for $n_g = 1/2$ is higher than that for $n_g = 0$. Whereas on the maximal-frustration line the system is in the superfluid state of the particle-void pairs even at small E_J , on the particle-hole symmetry line a sufficient amount of the Josephson energy is necessary for generating excitons, i.e., particle-hole pairs. For $n_g = 0.2$, the current mirror effect is indeed negligible and the increase in I_1 is also very small, as shown in Fig. 17(b).

V. CONCLUSION

We have studied phase transitions and persistent currents in a ladder of two capacitively coupled Josephson-junction necklaces. Emphasis has been paid on the roles of excitons in the presence of charge and magnetic frustration. To obtain the properties of the ground and excited states of the system, we have utilized the DMRG method for arbitrary values of the gate charge and of the magnetic flux. Although the main interest lies in the strong-coupling limit between the two necklaces, we have studied both the uncoupled and strongly coupled cases for comparison. In both cases, the gate voltage brings about crucial effects on the properties of the system. In a single Josephson-junction necklace, the presence of the gate voltage changes rather abruptly the behavior of the persistent current as well as nature of the phase transition. On the other hand, in the capacitively coupled Josephson-junction necklaces, such drastic change is not

observed but the gate voltage determines the class of excitons driving the phase transition: the particle-hole pairs near the particle-hole symmetry line and the particle-void pairs near the maximal-frustration line. In the presence of the Josephson tunneling, two different superfluid phases, characterized by the condensation of either of the two types of excitons, have been identified, depending on the gate charge. The pair correlation function and the exciton density have provided evidence for the formation of such excitons.

In the strongly coupled necklaces, the behavior of the persistent current is manifested by the competition between the current mirror effect and magnetic frustration, which is associated with the cotunneling transport of the bound excitonic pairs of either particles and holes or particles and voids. At small values of the Josephson energy, the current mirror effect wins the competition and only a very small amount of persistent current is allowed for a finite-sized system. At large values of the Josephson energy, magnetic frustration can make use of higher-charging-energy states to dominate over the current mirror effect, allowing a considerable amount of persistent current. We have also suggested an experimentally realizable system to demonstrate the cotunneling process of the excitons. To our present knowledge, the only experimental work related to the system considered here is that reported in Ref. 15. Unfortunately, however, the large bias voltage applied to both arrays does not allow us to make a direct connection. In particular our DMRG algorithm is not suitable for such a non-equilibrium problem.

Acknowledgments

We acknowledge the partial supports from the SKORE-A Program and from the BK21 Program.

* To whom correspondences should be addressed. E-mail: choims@korea.ac.kr

¹ See, e.g., *Single Charge Transport: Coulomb Blockade Phenomena in Nanostructures*, edited by H. Grabert and M. Devoret (Plenum Press, New York, 1992); D.V. Averin and K.K. Likharev, in *Mesoscopic Phenomena in Solids*, edited by B.L. Al'tshuler, P.A. Lee, and R.A. Webb (Elsevier Science, Amsterdam, 1991) p. 167.

² G. Schön and A.D. Zaikin, Phys. Rep. **198**, 237 (1990).

³ M.Y. Choi, Phys. Rev. B **48**, 15920 (1993).

⁴ R.M. Bradley and S. Doniach, Phys. Rev. B **30**, 1138 (1984); M.-S. Choi, J. Yi, M.Y. Choi, J. Choi, and S.-I. Lee, *ibid.* **57**, R716 (1998).

⁵ R. Fazio and G. Schön, Phys. Rev. B **43**, 5307 (1991).

⁶ A. van Otterlo, K.-H. Wagenblast, R. Fazio, and G. Schön, Phys. Rev. B **48**, 3316 (1993).

⁷ C. Giovannella and M. Tinkham (eds.) *Macroscopic Quantum Phenomena and Coherence in Superconducting Net-*

works (World Scientific, Singapore, 1995).

⁸ B.J. Kim and M.Y. Choi, Phys. Rev. B **52**, 3624 (1995); *ibid.* **56**, 395 (1997).

⁹ S. Sachdev, *Quantum Phase Transitions* (Cambridge Univ. Press, Cambridge, 1999), see also e-print cond-mat/9705266.

¹⁰ L.L. Sohn, L.P. Kouwenhoven, and G. Schön (eds.), *Mesoscopic Electron Transport* (Kluwer Academic Publishers, Dordrecht, 1997).

¹¹ In literature, “particles” and “holes” are used mostly to refer to elementary excitations in fermion systems. In this paper concerning about arrays of superconducting grains, we use them to refer to excess and deficit (boson-like) Cooper pairs rather than the constituent electrons.

¹² D.V. Averin, A.N. Korotkov, and Y.V. Nazarov, Phys. Rev. Lett. **66**, 2818 (1991).

¹³ M. Matters, J.J. Versluys, and J.E. Mooij, Phys. Rev. Lett. **78**, 2469 (1997).

- ¹⁴ M.-S. Choi, M.Y. Choi, T. Choi, and S.-I. Lee, Phys. Rev. Lett. **81**, 4240 (1998).
- ¹⁵ H. Shimada and P. Delsing, Phys. Rev. Lett. **85**, 3253 (2000).
- ¹⁶ E. Šimánek, *Inhomogeneous Superconductors: Granular and Quantum Effects* (Oxford Univ. Press, New York, 1994), p. 54.
- ¹⁷ R.A. Römer and M.E. Raikh, Phys. Rev. B **62**, 10455 (1999); J. Song and S.E. Ulloa, *ibid.* **63**, 125302 (2001); H. Hu, J.-L. Zhu, D.-J. Li, and J.-J. Xiong, *ibid.* **63**, 195307 (2001).
- ¹⁸ S.R. White and R.M. Noack, Phys. Rev. Lett. **68**, 3487 (1992); S.R. White, *ibid.* **69**, 2863 (1992); Phys. Rev. B **48**, 10345 (1993).
- ¹⁹ A. van Otterlo and K.-H. Wagenblast, Phys. Rev. Lett. **72**, 3598 (1994); A. van Otterlo, K.-H. Wagenblast, R. Baltin, C. Bruder, R. Fazio, and G. Schön, Phys. Rev. B **52**, 16176 (1995);
- ²⁰ T.D. Kühner, S.R. White, and H. Monien, Phys. Rev. B **61**, 12474 (2000).
- ²¹ J.K. Freericks and H. Monien, Europhys. Lett. **26**, 545 (1994); J.K. Freericks and H. Monien, Phys. Rev. B **53**, 2691 (1996).
- ²² R. Baltin and K.-H. Wagenblast, Europhys. Lett. **39**, 7 (1997).
- ²³ V.L. Berezinskii, Zh. Éksp. Teor. Fiz. **59**, 907 (1970) [Sov. Phys. JETP **32**, 493 (1971)]; J.M. Kosterlitz and D.J. Thouless, J. Phys. C **6**, 1181 (1973); J.M. Kosterlitz, J. Phys. C **7**, 1047 (1974); J.V. José, L.P. Kadanoff, S. Kirkpatrick, and D.R. Nelson, Phys. Rev. B **16**, 1217 (1977).
- ²⁴ M.Y. Choi, S.W. Rhee, M. Lee, and J. Choi, Phys. Rev. B **63**, 94 516 (2001).
- ²⁵ M.-S. Choi, M.Y. Choi, and S.-I. Lee, J. Phys.: Condens. Matter **12**, 943 (2000).
- ²⁶ M.Y. Choi and M. Lee, Curr. Appl. Phys. **2**, 11 (2002).